Scattering of neutral particles by an exponential corrugated potential: A solution for high corrugation amplitude

G. Armand
Centre d'Etudes Nucléaires de Saclay, Service de Physique des Atomes et des Surfaces, 91191 Gif-sur-Yvette Cedex, France

J. R. Manson
Department of Physics and Astronomy, Clemson University, Clemson, South Carolina 29631
(Received 7 August 1981)

For a two-dimensional exponential corrugated potential the scattering equation is solved to any desired accuracy. A distorted wave formalism is used in which the distorted (exponential) potential can be translated with respect to the corrugated potential. The integral-equation set is solved by the Neumann iterative process. It is shown that a suitable potential translation allows the extension of the convergence domain to high corrugation amplitudes. Thus the different particle-crystal systems encountered in experimental studies can now be analyzed with this soft potential. Compared to the hard corrugated wall potential the finite potential slope yields the following: (1) For small corrugation amplitude an enhancement of the specular intensity and a reduction of diffracted beam intensities. This reduction varies like the wave penetration. (2) For higher corrugation amplitude a shift of the rainbow maxima towards higher corrugation amplitude. The intensity maximum is enhanced or lowered according to whether the wave penetration of the diffracted beam is smaller or greater than that of the specular beam. In the case of the He-LiF system the emergence of the 01 beam is studied. With a potential sufficiently soft the singularities which appear around emerging conditions are smoothed. The measurement of their shape and amplitude could give an approximate value of the potential slope.

INTRODUCTION

The hard corrugated wall potential (HCWP) is widely used for the interpretation of thermal atomic beam diffraction experiments. In this model the repulsive potential part has an inifinite slope and therefore must be considered as an approximate representation of physical reality. Thus we have proposed recently[1,2] the so-called exponential corrugated potential (ECP), which is written as

$$V(\vec{R},z)=C\exp\{-\chi[z-\varphi(\vec{R})]\}\ . \tag{1}$$

As usual, z and $\vec{R}$ are, respectively, the normal and parallel components of a position vector, and $\varphi(\vec{R})$ is the corrugation function giving the surface periodicity.

The equipotential curves are obviously given by

$$z=\varphi(\vec{R})+\text{const}\ ,$$

and the potential slope

$$\frac{dV}{dz}=-\chi V(\vec{R},z) \tag{2}$$

has a finite value proportional to the range parameter χ. Note that the HCWP is recovered in the limit $\chi\to\infty$. These two potentials have the same equipotential curves, but having a finite slope the ECP can give an improved representation of the real potential.

Effectively the repulsive part of the potential is produced by the overlapping of the electronic wave functions of the incident atom with those of the crystal surface. Recently it has been demonstrated that the repulsive potential is, to a first approximation, proportional to the electron density near the surface.[3] Our choice of an exponential form is motivated by the fact that the density is expected to be exponential, and this has been confirmed by recent calculations[4] as well as by earlier determinations of the potential from first principles.[5,6] The attractive adsorption well near the surface can be explored by looking at the selective adsorption resonance phenomena. Knowing the positions of these resonances gives information on the zero-order Fourier component of the potential. However, the form of the well cannot be determined in a

unique way, and a large variety of potential shapes have been proposed; among them the 9-3, Morse, or shifted Morse hybrid potential are the most commonly used.[7]

With a purely repulsive potential such as (1) there is no possibility of studying the resonances; furthermore, if there is a well, the diffraction peaks are somewhat enhanced due to the fact that the particle strikes the corrugated wall with a higher effective energy. Nevertheless, apart from the regions of resonance one would expect Eq. (1) to represent well the effects of softness in the potential; in particular, at incident energies that are large compared to the well depth where very few resonances are observed experimentally. The authors have recently considered similar theoretical approaches for general forms of the potential that include a well and have substantiated the above-mentioned comments with calculations for a Morse potential.[8]

The potential of Eq. (1) does not contain any effects of the thermal vibration of the substrate atoms. In spite of the fact that these effects should be important at elevated temperatures one can compare the results of a purely elastic calculation with the elastic scattering data corrected for the Debye-Waller thermal attenuation. This has been done in a number of HCW calculations and, with the exception of certain resonance conditions, the agreement is quite favorable.[7] This situation should also hold when the repulsive part of the potential is replaced by a more natural soft wall such as that treated here.

The above considerations point out the usefulness of making diffraction amplitude calculations with more realistic potentials than the HCWP. Toward this objective we have solved the scattering equation with the ECP taking first a one-dimensional corrugation function.[1] Afterward the solution was extended to a two-dimensional surface.[2] With the numerical procedure adopted, reliable solutions were obtained for only small or medium corrugation amplitudes. We intend to present in this paper a procedure which extends the solution domain to high corrugation amplitude. Thus all cases of practical interest in atom surface scattering can be now calculated. In addition, new physical results are presented, which, when compared to HCWP results, illustrate the effect of wave penetration into the potential.

T-MATRIX INTEGRAL EQUATIONS—INTENSITIES

In the two-potential or distorted-wave formalism the integral form of the Schrödinger equation appears as

$$|\psi_i^+\rangle = |\phi_i\rangle + (E_i - H_0 + i\epsilon)^{-1} \times [V(\vec{R},z) - W]\,|\psi_i^+\rangle \qquad (3)$$

with the Hamiltonian H_0 given by

$$H_0 = -\frac{\hbar^2}{2m}\nabla^2 + W ,$$

where $V(\vec{R},z)$ is the interaction potential and W the distorted potential.

The direction $\vec{0}_z$ is normal to the surface. A wave or a position vector $(\vec{k},\vec{r})$ is decomposed into components parallel $(\vec{K},\vec{R})$ and normal (k_z,z) to the surface.

The shape of the potential $V(\vec{R},z)$ is imposed by the nature of the interaction between the incident particle and the surface. We suppose here that V is a continuous decreasing function of z: There is no potential well. With only elastic scattering, V has the periodicity of the surface unit cell. Therefore it can be decomposed into the Fourier expansion

$$V(\vec{R},z) = \sum_{\vec{G}} v_{\vec{G}}(z)\exp[i(\vec{G}\cdot\vec{R})] ,$$

where $\vec{G}$ is a surface reciprocal-lattice vector and

$$v_{\vec{G}}(z) = \frac{1}{S}\int_{UC} d\vec{R}\, V(\vec{R},z)\exp[-i(\vec{G}\cdot\vec{R})d\vec{R}] , \qquad (4)$$

with S the area of the unit cell (UC).

As for W, the choice is quite arbitrary. Thus it is most interesting to chose a form which is convenient for solving Eq. (3). With this in mind W is taken as a function of z only, as close as possible to V, and in such a way that the continuous set of eigenvalues $\hbar^2K^2/2m + e_p$ and eigenfunctions $e^{i\vec{K}\cdot\vec{R}}\phi_p(z)$ of H_0 are known. Letting

$$\int_{-\infty}^{+\infty} \phi_q^*(z)\phi_p(z)dz = B^2\delta(p-q) ,$$

a lengthy but straightforward calculation detailed in Ref. 2 gives the set of integral equations obeyed by a set of functions denoted by $L_J(s)$ which are, apart from a normalization factor, equal to the reduced t-matrix element

$$t_{\vec{J}_i}(s) = \langle \exp[i(\vec{K}_i + \vec{J})\cdot\vec{R}]\phi_s(z)\,|\,V(\vec{R},z) - W(z)\,|\,\psi_i^+\rangle .$$

One gets

$$L_{\vec{J}}(s)=\frac{1}{B^2}\left[N_{\vec{J}-\vec{0}}(s,p_i)-\delta_{\vec{J}\,\vec{0}}M(s,p_i)+\sum_{\vec{G}}\int_0^\infty dq\frac{[N_{\vec{J}-\vec{G}}(s,q)-\delta_{\vec{J}\,\vec{G}}M(s,q)]L_{\vec{G}}(q)}{E_i-(\hbar^2/2m)(\vec{K}_i+G)^2-e_q+i\epsilon}\right], \tag{5}$$

with

$$N_{\vec{J}-\vec{G}}(s,q)=\int_{-\infty}^{+\infty}\phi_s^*(z)v_{\vec{J}-\vec{G}}(z)\phi_q(z)dz\ ,$$
$$M(s,q)=\int_{-\infty}^{+\infty}\phi_s^*(z)W(z)\phi_q(z)dz\ .$$

The subscript i denotes, as usual, the incident state.

With the Fourier components of the exponential corrugated potential (1) being given by

$$v_{\vec{G}}(z)=Cv_{\vec{G}}\exp(-\chi z)$$

with

$$v_{\vec{G}}=\frac{1}{S}\int_{UC}\exp(-i\vec{G}\cdot\vec{R})\exp[\chi\varphi(\vec{R})]d\vec{R}$$

and S the area of the unit cell, one takes for $W(z)$ an equivalent form, namely

$$W(z)=Dv_{\vec{0}}\exp(-\chi z)\ .$$

In the previous work[1,2] the undefined constant D was taken in such a way that $Dv_{\vec{0}}=C$. Here different values of D and C allow us to translate the potential $W(z)$ with respect to V as we can write

$$W(z)=Cv_{\vec{0}}\exp[-\chi(z-l)]\ .$$

For further simplification we write

$$\frac{D}{C}=\beta=\exp(\chi l)\ .$$

If $\beta=1$ the potential $W(z)$ coincides with the zero-order Fourier component of the corrugated potential.

The eigenvalues of H_0 are given by[9]

$$e_p=\frac{(\hbar\chi)^2}{8m}p^2\ ,\quad p=2\frac{k_z}{\chi}\ ,$$

and the eigenfunctions are

$$e^{i\vec{K}\cdot\vec{R}}\phi_p(z)=e^{i\vec{K}\cdot\vec{R}}\left[\frac{p\sinh(\pi p)}{\pi}\right]^{1/2}K_{ip}(y)\ ,$$

$$y=\frac{(8mDv_0)^{1/2}}{\chi\hbar}\exp\left[\frac{-\chi z}{2}\right],$$

where K_{ip} is the modified Bessel function of the second kind of imaginary order ip.

Now the different quantities which enter into Eq. (5) have already been calculated. The detailed presentation being given in Ref. 2, we give only the final result. Setting

$$F_{\vec{J}}(s)=\frac{16m}{(\hbar\chi)^2}L_{\vec{J}}(s)$$

one gets

$$F_{\vec{J}}(s)=\lambda_{\vec{J}\,\vec{0}}f(s,p_i)+\frac{1}{2}\sum_{\vec{G}}\lambda_{\vec{J}-\vec{G}}\int_0^\infty dq\frac{f(s,q)F_{\vec{G}}(q)}{p^2_{\vec{G}}-q^2+i\epsilon}\ , \tag{6a}$$

or in matrix form,

$$\underline{F}_{\vec{J}}(s)=f(s,p_i)\underline{\lambda}_{\vec{J}\,\vec{0}}+\frac{1}{2}\underline{\lambda}_{\vec{J}-\vec{G}}\int_0^\infty dq\, f(s,q)(\underline{M})_d^{-1}\underline{F}_{\vec{G}}(q)\ , \tag{6b}$$

where $\underline{M}=(p^2_{\vec{G}}-q^2+i\epsilon)$. In Eq. (6) the different quantities are given by

$$\lambda_{\vec{J}-\vec{G}}=\frac{v_{\vec{J}-\vec{G}}}{v_{\vec{0}}\beta}-\delta_{\vec{J}\,\vec{G}}\ , \tag{7}$$

$$f(s,q)=\begin{cases}[s\sinh(\pi s)q\sinh(\pi q)]^{1/2}\dfrac{s^2-q^2}{\cosh(\pi s)-\cosh(\pi q)}\ , & s\neq q\\ \dfrac{2}{\pi}q^2\ , & s=q\end{cases} \tag{8}$$

$$p^2_{\vec{G}}\equiv\frac{4}{\chi^2}[\,|k_i|^2-(\vec{K}_i+\vec{G})^2]\equiv\frac{4}{\chi^2}(k_{\vec{G}\,z})^2\ .$$

It has been shown[2] that the partial wave function corresponding to each diffracted beam is a sum of one plane wave and many exponentially damped waves for an open channel. For a closed channel the wave function contains only exponentially damped waves. Taking the limit $z \to \infty$ one finds the wave amplitude, which is given by

$$A_{\vec{J}} = i\delta_{\vec{J}\,0} - \frac{\pi}{2}\frac{F_{\vec{J}}(p_{\vec{J}})}{p_{\vec{J}}} . \tag{9}$$

The reflection coefficient for each open channel is then easily calculated:

$$R_{\vec{J}} = k_{\vec{J}z}(k_{iz})^{-2}|A_{\vec{J}}|^2 .$$

The solution of the set of equations (6) allows one to determine directly the reflection coefficients.

NUMERICAL METHODS OF SOLUTION

The solution of equations (6) is easily found in the following particular cases:

(i) $\varphi(\vec{R}) \equiv 0$; that is, for a potential without a corrugation. This implies $\lambda_{\vec{J}-\vec{G}} = 0$ ($\beta = 1$) and $F_{\vec{J}}(s) \equiv 0$, whatever $\vec{J}$ may be.

(ii) The incident angle is equal to 90°. In this case $p_i = 0$ and $f(s,p_i) \equiv 0$ which gives $F_{\vec{J}}(s) \equiv 0 \forall \vec{J}$.

In these two cases the particles are completely reflected into the specular beam.

Except for particular cases it is necessary, in all situations of practical interest, to solve the set of equations by a numerical procedure. Whatever the chosen procedure may be, one can keep only a finite number of reciprocal vectors $n_{\vec{G}}$, this set including at least all the vectors corresponding to the open channels. In addition, the integration over the q variable must be carried out on an interval $[0,q_M]$, q_M being substantially greater than the largest value of the real $p_{\vec{G}}$ number set. However, it is not necessary to ascribe to q_M a very large value because the integrand is proportional to $\exp(-\pi q)$ for large q. In effect, for large s, $f(s,q)$ is proportional to $\exp[-(\pi/2)s]$ and $F_{\vec{J}}(s)$ is consequently proportional to this same factor. Therefore the product $f(s,q)F_G(q)$ is of the order of $\exp(-\pi q)$.

Two classes of numerical processes can be considered. In the first, the set of equations (6) is transformed into a discrete set of linear equations. This can be achieved in different ways:

(a) Each principal-part integral is transformed into a sum of values taken by integrands at the special points of the interval $[0,q_M]$. This procedure has been used in order to solve the integral equation of the HCWP with a two-dimensional surface.[10] Compared to a partition of the interval by a set of equally spaced points,[1] the number of points necessary to achieve a given precision is reduced by this special choice. However, if n is the number of points, the dimension of the matrix to be inverted is equal to $n_{\vec{G}} \times n$ and generally will exceed the computer capacity available to date.

(b) The $F_{\vec{J}}(s)$ functions are expanded in an infinite set of Laguerre polynomials. Retaining n_L Laguerre coefficients, this leads again to a large matrix equation.

(c) The kernel $f(s,q)$ in Eq. (6) is transformed into a degenerate kernel,[11] for instance, by a double Fourier cosine expansion. In this case we have again the problem of solving a very large system of linear equations.

In the second class of solutions one uses the Neumann iterative process. To this class belongs the solutions by means of the reaction matrix (R or K) the iteration being used to obtain these matrix elements. After that a matrix inversion gives the t-matrix element values. In this way the result is always unitary, a condition which is not sufficient to warrant that the solution obtained is the correct one. Note that the so called Cabrera-Celli-Goodman-Manson (CCGM) approximation,[12] which consists of neglecting the principal-part integral, corresponds to the first iteration step of the R matrix[13] for the potential used in this paper. At first sight an iteration of the t-matrix equations themselves seems to be less expensive in computer time and permits easy control on the validity of the result obtained. As we intend to use this method, it is necessary to study the convergence of the iterative process.

CONVERGENCE STUDY OF THE ITERATIVE PROCESS ON t-MATRIX EQUATIONS

In the case of a system of integral equations in which the $\lambda_{\vec{J}-\vec{G}}$ coefficients are all equal, the convergence radius can be analytically determined.[11] In our case the $\lambda_{\vec{J}-\vec{G}}$ are all different and given by Eq. (7) in which β is a parameter taking values in the range $0- + \infty$. Therefore $\lambda_{\vec{J}=\vec{G}}$ and $\lambda_{\vec{J}-\vec{G}}$ can vary, respectively, from ∞

to -1 and ∞ to 0 over the range of β.

For given initial conditions there is probably an interval in which the iterative solution is convergent, and it is interesting to write its analytical form in order to determine at least qualitatively the range of good β values. Starting the iteration with any integrable function $h_{\vec{J}}(s,p_i)$ we obtain

$$F^{(0)}_{\vec{J}}(s)=h_{\vec{J}}(s,p_i)\ ,$$

$$F^{(1)}_{\vec{J}}(s)=\lambda_{\vec{J}\,0}f(s,p_i)+\tfrac{1}{2}\sum_{\vec{G}_1}\lambda_{\vec{J}-\vec{G}_1}\int_0^\infty dq_1 h_{\vec{G}_1}(q,p_i)K^{(1)}_{\vec{G}_1}(s,q)\ ,$$

with

$$K^{(1)}_{\vec{G}_1}(s,q)=(p^2_{\vec{G}_1}-q^2+i\epsilon)^{-1}f(s,q)\ , \tag{10}$$

$$F^{(2)}_J(s)=\lambda_{\vec{J}\,0}f(s,p_i)+\tfrac{1}{2}\sum_{\vec{G}_1}\lambda_{\vec{J}-\vec{G}_1}\lambda_{\vec{G}_1 0}\int_0^\infty dq\,K^{(1)}_{G_1}(s,q)f(q,p_i)$$

$$+\tfrac{1}{4}\sum_{\vec{G}_2}\sum_{\vec{G}_1}\lambda_{\vec{J}-\vec{G}_2}\lambda_{\vec{G}_2-\vec{G}_1}\int_0^\infty dq\,K^{(2)}_{\vec{G}_2\vec{G}_1}(s,q)h_{\vec{G}_1}(q,p_i)\ ,$$

with

$$K^{(2)}_{\vec{G}_2\vec{G}_1}(s,q)=(p^2_{G_1}-q^2+i\epsilon)^{-1}\int_0^\infty dq_2\frac{f(s,q_2)f(q_2,q)}{p^2_{G_2}-q_2^2+i\epsilon}=\int_0^\infty\frac{dq_2 f(s,q_2)}{p^2_{\vec{G}_2}-q_2^2+i\epsilon}K^{(1)}_{G_1}(q_2,q)\ , \tag{11}$$

and so on. For the nth step one gets

$$F^{(n)}_{\vec{J}}(s)=\lambda_{\vec{J}\,0}f(s,p_i)+\int_0^\infty dq\,f(q,p_i)$$

$$\times\left[\sum_{p=1}^{n-1}2^{-p}\left(\sum_{\vec{G}_p}\sum_{\vec{G}_{p-1}}\cdots\sum_{\vec{G}_1}\lambda_{\vec{J}-\vec{G}_p}\lambda_{\vec{G}_p-\vec{G}_{p-1}}\cdots\lambda_{\vec{G}_1 0}\right)K^{(p)}_{\vec{G}_p\cdots\vec{G}_1}(s,q)\right]$$

$$+2^{-n}\sum_{\vec{G}_n}\sum_{\vec{G}_{n-1}}\cdots\sum_{\vec{G}_1}\lambda_{\vec{J}-\vec{G}_n}\lambda_{\vec{G}_n-\vec{G}_{n-1}}\cdots\lambda_{\vec{G}_2-\vec{G}_1}\int_0^\infty dq\,K^{(n)}_{\vec{G}_n\vec{G}_{n-1}\cdots\vec{G}_1}(s,q)h_{\vec{G}_1}(q,p_i)\ ,$$

with $K^{(1)}$ and $K^{(2)}$ given, respectively, by (10) and (11), and

$$K^{(p)}_{\vec{G}_p\cdots\vec{G}_1}(s,q)=\int_0^\infty\frac{f(s,q_p)}{p^2_{\vec{G}_p}-q_p^2+i\epsilon}K^{(p-1)}_{\vec{G}_{p-1}\cdots\vec{G}_1}(q_p,q)dq_p\ .$$

One sees immediately that the convergence or divergence of $F^{(n)}_{\vec{J}}(s)$ as n increases depends upon the convergence or divergence of the expansion contained in the square brackets. The $F^{(n)}_{\vec{J}}(s)$ behavior is not dependent upon the form of the starting function $h_{\vec{J}}(s,p_i)$, as it enters only in the last term. For the given kernels $f(s,q)(p^2_G-q^2+i\epsilon)^{-1}$ the $K^{(p)}$ functions are determined, and the convergence depends only the $\lambda_{\vec{J}-\vec{G}}$ values, that is to say on β for a given physical system. At first sight and in the case of real $\lambda_{\vec{J}-\vec{G}}$ coefficients it seems interesting to reduce the $\lambda_{\vec{J}-\vec{G}}$ values by taking β greater than 1. Doing so the $\lambda_{\vec{J}=\vec{G}}$ coefficient becomes negative, and then some cancellation between the different terms of the expansion may occur. A more precise argument valid even for complex coefficients is outlined below.

The numerical calculation confirms this view and allows one to estimate the convergence domain. It has been carried out for the same conditions of previous work[2] corresponding to a hydrogen molecule ($|k_i|=8.6$ Å^{-1}) scattered by a copper (100) surface ($a=2.55$ Å). The incident plane contains the [100] direction and the incident angle θ_i with respect to the normal is equal to 31° or 60.5°, giving, respectively, 37 or 39 open channels. The corrugation function is taken as

$$\varphi(\vec{R})=\tfrac{1}{2}ha\left[\cos\left[\frac{2\pi x}{a}\right]+\cos\left[\frac{2\pi y}{a}\right]\right], \quad (12)$$

and the Fourier components v_G are equal to

$$v_G=I_{G_x}(\chi ha/2)I_{G_y}(\chi ha/2),$$

$$\vec{G}=(G_x\vec{0}_x,G_y\vec{0}_y)\frac{2\pi}{a},$$

with I the modified Bessel function of the first kind.

As in the previous work the convergence (or divergence) of the iterative process is estimated by comparing to unity the sum of all diffracted beam intensities U, hereafter called the unitary sum. For a convergent process the unitary defect $\Delta^{(n)}=|U^{(n)}-1|$ should decrease from one iteration step to another provided a sufficiently large number of iterations is considered. In addition, all other parameters remaining the same, the $\Delta^{(n)}$ should be smaller if the number of reciprocal-lattice vectors retained in the calculation is increased. These criteria lead us to consider as divergent an iteration in which the unitary defect first approaches a value close to zero, but after that slowly increases as the iteration process is continued. This type of behavior is sometimes referred to as asymptotic convergence.

It is worthwhile to note that the different numerical calculations should be made with sufficient precision. This point is valid particularly for the different principal-value integrations that can be carried out following a procedure developed in Ref. 2. Given the numerical procedure, the integration step should be chosen carefully. All the calculations were done on a CDC 7600 computer that works with 16 significant figures in single precision.

All the results with respect to convergence or divergence are plotted in Fig. 1. To each case corresponds a point in the coordinate plane $\lambda_{00}=\beta^{-1}-1$ vs $\lambda_{01}=v_{01}(v_{00}\beta)^{-1}$, the most important $\lambda_{\vec{J}-\vec{G}}$ coefficients. For a given value of $\gamma=\chi ha/2$ there is a linear relation between these two coefficients. The representative point of a given trial moves along a line corresponding to a particular value of γ when β varies. The straight line with negative slope is the locus of points for which $-\lambda_{00}=\lambda_{01}$.

A point labeled with a letter D corresponds to a divergent process; a point without a label corresponds to a convergent iteration. Thus the

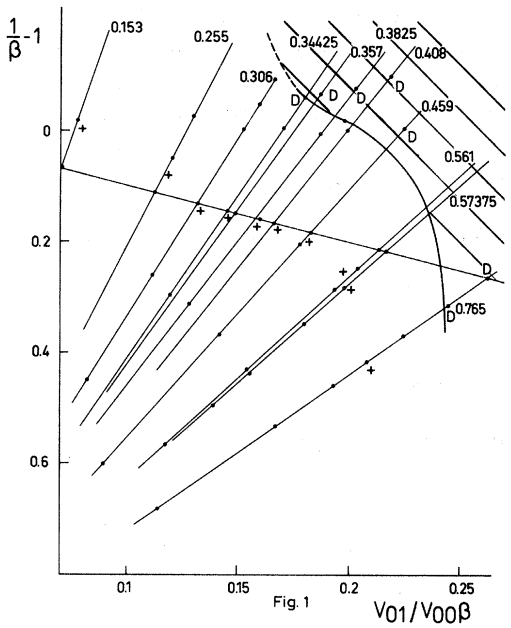

Fig. 1

FIG. 1. Convergence diagram. $\lambda_{00}=1/\beta-1$, $\lambda_{01}=V_{01}/V_{00}\beta$.

shaded area is the region of divergence. In the convergence region for each γ value a cross labels the point for which the iteration process converges the fastest, that is, the point for which a given unitary defect is reached with the least number of iterations. For a unitary defect of the order of 10^{-3} to 10^{-4} this number increases with γ, going from 10 to 40 in the explored γ range and the relative translation of the two potentials l increases from 0 to about $0.7ha$. For the same γ value the number of iterations required is a little smaller for large χ, due certainly to the fact that the dimensionless $p_{\vec{G}}$ numbers are then smaller.

In previous work[2] with $Dv_{\vec{0}}=C$, the convergence holds for γ values less than 0.34. Here the convergence domain is larger and *a priori* not limited, although we do not try to go beyond a γ value equal to 0.765. To this case corresponds the pair $h=0.04$ and $\chi=15$ Å^{-1}, giving, as we will see below, the HCWP limit and the pair $h=0.2$ $\chi=3$ Å^{-1}. This last h value is certainly a high corrugation amplitude in comparison with the various crystal surfaces studied to date. Thus the present results allow the possibility of obtaining a good solution in virtually all practical cases encountered in surface scattering.

As the convergence diagram depends upon the variables λ_{00} and λ_{01} it should be good for any corrugation shape for which the two first Fourier components of the corrugation are the most impor-

tant. This is certainly true in the region of small λ_{01} values where the higher-order λ coefficients are negligible. In the region of high λ_{01} values the convergence diagram shape should be perhaps slightly different for different types of corrugations due to the influence of other λ coefficients. Of course the $\gamma=$const straight line would be different as well as the points that give the fastest convergence.

Therefore, it is interesting to try to go deeper into the understanding of the convergence domain. In order to do so we consider the matrix integral equation (6b). The square matrix $\underline{\lambda}_{\vec{J}-\vec{G}}$ is Hermitian and can be written

$$\underline{\underline{\lambda}}_{\vec{J}-\vec{G}}=\underline{\underline{B}}^{+}\underline{\underline{\omega}}\,\underline{\underline{B}}$$

with ω its real eigenvalues and $\underline{B}$ a unitary matrix. A similarity transformation leads to the new matrix integral equation:

$$\underline{H}_n(s)=f(s,p_i)\underline{h}_n+\tfrac{1}{2}(\underline{\omega}_n)_d\int_0^{\infty}dq\,f(s,q)\underline{\underline{G}}_{nm}(q)\underline{H}_m(q)\ , \quad (13)$$

with

$$\underline{H}_n(s)=\underline{\underline{B}}\,\underline{F}_{\vec{J}}(s)\ ,\quad \underline{h}_n=\underline{\underline{B}}\underline{\lambda}_{\vec{J}0}\ ,$$

and

$$\underline{\underline{G}}_{nm}(q)=\underline{\underline{B}}(\underline{\underline{M}})_d^{-1}\underline{\underline{B}}^{+}\ ,$$

which has the form of a Green matrix.

The new unknown $H_n(s)$ functions are equivalent to a linear combination of the $F_{\vec{J}}(s)$ functions. One can think that if by an iterative process the convergence is reached with one of the two matrix equations the iteration will be convergent with the other and vice versa.

Here with Eq. (13) the parameters that govern the iteration behavior are the eigenvalues ω_n. The pth iteration step is written as

$$\underline{H}_n^{(p)}(s)=\underline{H}_n^{(p-1)}(s)+\frac{1}{2^p}\left[\prod_{r=2}^{p}\left[(\underline{\omega}_r)_d\int_0^{\infty}dq_r f(q_{r+1},q_r)\underline{\underline{G}}(q_r)\right]\right](\underline{\omega}_1)_d\int_0^{\infty}dq_1 f(q_2,q_1)\underline{\underline{G}}(q_1)f(q_1,p_i)\underline{h}_m\ ,$$

which shows that the pth iteration result is obtained by adding to the $(p-1)$th a sum of terms, each being given by the result of a multiple integration (of order p) multiplied by the product of p eigenvalues ω_n. In order to get a convergent process it would certainly be interesting to reduce their absolute values and also probably to take a β value in such a way that the ω_n numbers should be roughly evenly distributed about zero. With this condition some terms in the sum will be positive, others will be negative, and cancellation may occur.

This view can be substantiated in the following way. Let us suppose that the λ coefficients are real and equal to zero except λ_{00}, $\lambda_{01}=\lambda_{10}=\lambda_{0\bar{1}}=\lambda_{\bar{1}0}>0$. The $\lambda_{\vec{J}-\vec{G}}$ matrix appears as

$$\begin{vmatrix}
\lambda_{00} & \lambda_{01} & \lambda_{01} & 0 & & \\
\lambda_{01} & \lambda_{00} & \lambda_{01} & \lambda_{01} & 0 & \\
\lambda_{01} & \lambda_{01} & \lambda_{00} & \lambda_{01} & \lambda_{01} & 0 \\
0 & \lambda_{01} & \lambda_{01} & \lambda_{00} & \lambda_{01} & \lambda_{01} \\
 & & & & \ddots &
\end{vmatrix}\ . \quad (14)$$

It is shown in the Appendix that the eigenvalues ω_n are given by

$$\omega_n=\lambda_{00}-2\lambda_{01}\left[1+\cos\frac{k\pi}{N+1}-2\cos^2\left[\frac{k\pi}{N+1}\right]\right]\ ,$$

with N the matrix size, provided N is large. Therefore the ω_n values lie in the interval

$$\lambda_{00}-\tfrac{9}{4}\lambda_{01}<\omega_n<\lambda_{00}+4\lambda_{01}\ .$$

Figure 1 indicates that the divergences appears for $\lambda_{01}>0.2$ when $\lambda_{00}=0$. Then we have $-0.45<\omega_n<0.8$.

For conditions in which the convergence in achieved faster we have $\lambda_{00}=-\lambda_{01}$, and therefore

$$-3.25\lambda_{01}<\omega_n<3\lambda_{01}\ .$$

This result illustrates and confirms our earlier intuition: The convergence is achieved and is faster when the eigenvalues ω_n are distributed roughly symmetrically about zero and have the smallest possible absolute values. This criteria always seems to be good even in the case of complex $\lambda_{\vec{J}-\vec{G}}$ coefficients. Then the knowledge of the ω values allows one to predict the behavior of the iteration process.

VARIATION OF POTENTIAL RANGE PARAMETER OR CORRUGATION AMPLITUDE

All the results presented in this section have been obtained for H_2-Cu(100) under the same conditions depicted in the preceding section. Of course, due to the symmetry of the chosen incident conditions, one always find $R_{G_x,G_y}=R_{G_y,G_x}$.

We first consider a variation of χ taking h constant and equal to 0.04. Tables I and II give the calculated reflection coefficients for incident angles θ_i of 31° and 60.5°. Also given are the intensities calculated with the HWCP using the *NN* special point method, which was treated elsewhere,[10] and the E_Z values, which are equal to the ratio of the normal kinetic energy of the beam to that of the specular beam. One can observe readily the following facts:

(1) When χ increases the HCWP intensities are approached as expected. The 00 beam intensity decreases and is always greater than the corresponding HCWP intensity. The converse is true for the diffracted beams if one excepts the $0\bar{1},\bar{1}0$ at $\theta_i=31°$, which reaches its maximum value in the vicinity of $\chi=5$ Å^{-1}. However, beyond this value its variation is not important.

(2) All the beam intensities vary rapidly for low χ values, more precisely for $\chi<3$ Å^{-1}. Above this value the variation is smoother. However, considering the diffracted beams the relative difference between intensities given by the ECP and the HCWP is smaller for beams which have a greater normal kinetic energy than the specular beam ($E_Z>1$).

A second set of calculations was made at constant χ (3 Å^{-1}) and for an incident angle of 3°1 with h varying from 0 to 0.18. The results are depicted in Fig. 2; each curve is labeled by two numbers giving, respectively, the diffracted beam order and its corresponding E_Z value. For comparison Fig. 3 gives the intensity evolution under the same conditions in the case of the HCWP. Figure 4 gives the specular beam variation.

The rainbow effect is clearly apparent in these figures. Comparison between the two potential results indicates that the peak maximum are shifted towards higher corrugation with the soft potential ($\chi=3$ Å^{-1}). Table III illustrates quantitatively this effect. The shift is of the order of $\Delta h=0.012-0.015$ except for the 11 beam, which has a very small normal kinetic energy and for which the shift is certainly much more important. One notices too that the intensity maxima are greater with the ECP when the diffracted beam has a normal kinetic energy greater than that of the specular beam. When this is not the case, the reverse happens, the $\bar{2}1$ beam being an exception to this rule. As far as the 00 beam is concerned the intensity given by the soft potential is always greater. The hard potential yields an intensity minimum at h about 0.15. Above this value the intensity probably increases and the rainbow effect will appear for very high corrugation amplitude.

EMERGING BEAM

For a given system a diffracted beam can emerge, for instance, when the incident angle θ_i is made to vary. This means that the beam passes

TABLE I. Reflection coefficients of the most significant beams for the H_2-Cu(001) system as a function of χ. HCWP corresponds to infinite χ. E_Z is the normal kinetic energy ratio of the beam to that of the specular beam. $|k_i|=6.8$ Å^{-1}, $a=2.55$ Å, $h=0.04$, $\theta_i=31°$, $\varphi=45°$.

χ (Å^{-1})	1	3	5	6	7	8	9	11	15	HCWP	E_Z
R_{00}	0.903 75	0.695 81	0.629 40	0.614 53	0.604 94	0.598 47	0.593 93	0.588 17	0.583 45	0.578 00	1
$R_{11}\times10^2$	0.16×10^{-6}	0.038 16	0.187 81	0.253 71	0.305 19	0.344 62	0.374 30	0.414 00	0.449 76	0.472 85	0.208
$R_{10}\times10$	0.37×10^{-2}	0.367 17	0.618 83	0.678 57	0.717 35	0.743 70	0.762 03	0.785 42	0.809 50	0.824 37	0.604
$R_{1\bar{1}}\times10$	0.41×10^{-3}	0.0492	0.088 3	0.097 98	0.104 38	0.108 73	0.111 82	0.115 75	0.118 84	0.122 72	0.776
$R_{0\bar{1}}\times10$	0.4326	0.967 67	0.987 99	0.987 31	0.986 14	0.984 99	0.984 09	0.982 99	0.936 68	0.980 33	1.172
$R_{\bar{1}\bar{1}}\times10$	0.0276	0.163 02	0.185 89	0.189 76	0.192 09	0.193 57	0.194 63	0.195 89	0.196 92	0.198 13	1.344
$R_{\bar{1}\bar{2}}\times10^3$	0.1921	0.7680	0.849 89	0.863 75	0.872 24	0.877 54	0.880 98	0.885 38	0.854 33	0.896 14	1.29
$R_{1\bar{2}}\times10^3$	0.0027	0.1904	0.312 89	0.341 90	0.360 84	0.373 51	0.382 40	0.393 88	0.390 27	0.414 3	0.725
U	1.000 00	0.999 99	0.999 99	0.999 99	0.999 99	1.000 01	0.999 97	1.000 03	.1001 84	0.999 49	

TABLE II. Same as Table I but $\theta_i = 60.5$.

χ (Å^{-1})	1	3	5	6	8	9	11	15	HCWP	E_Z
R_{00}	0.999 88	0.959 57	0.916 96	0.905 11	0.891 34	0.887 31	0.882 15	0.877 80	0.874 66	1
$R_{0\bar{1}} \times 10$	0.583×10^{-3}	0.190 46	0.382 09	0.434 04	0.493 70	0.511 07	0.553 20	0.533 88	0.555 83	2.11
$R_{\bar{1}\bar{1}} \times 10^2$	0.63×10^{-5}	0.110 36	0.357 04	0.442 82	0.550 69	0.583 75	0.627 56	0.665 30	0.687 72	3.23
$R_{1\bar{1}} \times 10^3$	0.31×10^{-4}	0.088 94	0.364 95	0.486 44	0.653 15	0.705 94	0.771 34	0.817 10	1.286 86	0.322
$R_{0\bar{2}} \times 10^2$	0.65×10^{-4}	0.047 71	0.100 30	0.114 79	0.131 60	0.136 50	0.142 76	0.147 17	0.147 81	2.55
$R_{\bar{1}\bar{2}} \times 10^2$	0.14×10^{-5}	0.040 27	0.129 81	0.160 47	0.197 05	0.208 20	0.223 29	0.229 70	0.258 43	3.67
U	1.000 00	1.000 00	0.999 99	0.999 99	0.999 99	0.999 99	0.999 98	1.000 32	0.999 07	

from the state of an evanescent wave to an observable diffracted peak. Let us suppose that the beam corresponding to a reciprocal-lattice vector $\vec{M}$ emerges for an incident angle $\theta_{\vec{M}}$. If θ_i decreases in the vicinity of $\theta_{\vec{M}}$, the value of $p^2_{\vec{M}}$, which is negative, will pass through zero at $\theta_{\vec{M}}$ and become positive. In Eq. (6a) this yields a δ function $\delta(p^2_{\vec{M}} - q^2)$ in the sum over the reciprocal-lattice vector as soon as $p^2_{\vec{M}}$ becomes positive. One can then expect to observe in each diffracted beam intensity a disturbance in the vicinity of $\theta_i = \theta_{\vec{M}}$.

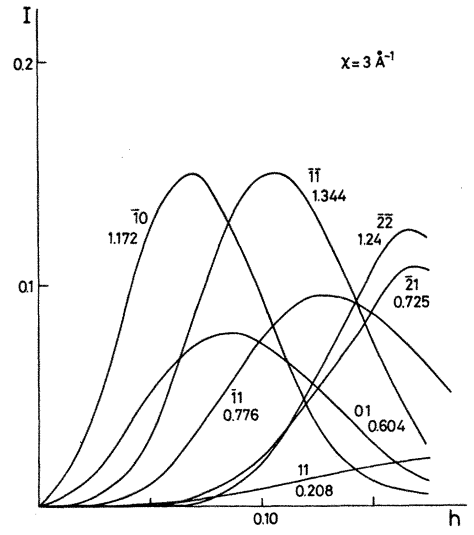

FIG. 2. Evolution of beam intensities as a function of corrugation amplitude given by the exponential corrugated potential. Each curve is labeled with the beam order and E_Z number, which is equal to the ratio of the normal kinetic energy of the beam to that of the specular beam. The system is H_2-Cu(001) with $|k_i| = 6.8$ Å^{-1}, $a = 2.55$ Å, $\theta_i = 31°$, $\varphi = 45°$.

This effect should certainly be the greatest for a beam $\vec{J}$ having the largest potential Fourier component $v_{\vec{J}-\vec{M}}$, that is, for those which are strongly coupled with the emerging beam. Therefore the disturbance will be important for the emerging beam itself and for those having a $\vec{J}$ vector close to $\vec{M}$. As the Fourier component of the potential increases with χ the disturbance will become more and more important and will be maximum in the HCWP case.

A result which illustrates this effect has been given in a previous paper[2] with the same beam-crystal system used in the previous sections. Under these conditions at $\theta_{\vec{M}} = 50.96°$ the 01 and 10 beams are simultaneously emerging. Calcula-

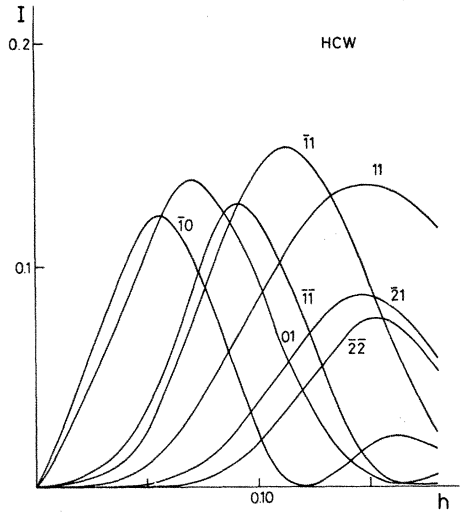

FIG. 3. Evolution of beam intensities as a function of corrugation amplitude given by the hard corrugated wall for the same system as Fig. 2. Each curve is labeled with the beam order.

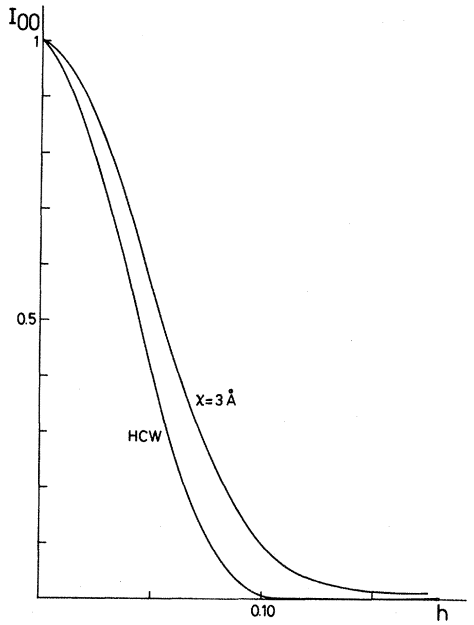

FIG. 4. Evolution of the specular intensity as a function of corrugation amplitude for the hard corrugated wall (HCWP) and the exponential corrugated potential (3 $Å^{-1}$) for the same system as Fig. 2.

tion indicates that the disturbance is very important with regard to the 00 and $1\bar{1}$ beams and is less apparent with the others. Its magnitude is the greatest in the HCWP case but completely disappears with the ECP for $\chi=3$ $Å^{-1}$. However, the derivative of the emerging beam intensity versus incident angle is very large at $\theta_i=\theta_{\vec{M}}$ in any case.

Here we present another example of this effect. We consider a helium beam scattered by the (001) face of lithium fluoride. The incident plane contains the [110] direction. For the 01 and 03 beams

TABLE III. Position h_m of the intensity maximum I_m for the most significant beams for H_2 incident on a Cu(100) surface. E_Z is the normal kinetic energy ratio of the beam to that of the specular beam. $|k_i|=6.8$ $Å^{-1}$, $a=2.55$ Å, $\theta_i=31°$, $\varphi=45°$.

		$\chi\to\infty$ (HCWP)		$\chi=3$ $Å^{-1}$	
Beam	E_Z	h_m	I_m	h_m	I_m
$\bar{1}\bar{1}$	1.344	0.09	0.128	0.107	0.150
$2\bar{2}$	1.24	0.152	0.077	0.167	0.125
$\bar{1}0$	1.172	0.056	0.123	0.07	0.150
$\bar{1}1$	0.776	0.113	0.153	0.128	0.095
$\bar{2}1$	0.725	0.148	0.087	0.17	0.108
01	0.604	0.07	0.139	0.085	0.088
11	0.208	0.15	0.137	>0.18	

the $\theta_{\vec{M}}$ angles are, respectively, 53.02° and 52.89°. The Ewald diagram is drawn in Fig. 5. We take for this calculation a χ value of 3 $Å^{-1}$ and corrugation which gives, in the framework of HCWP, the best fit between calculated and measured intensity of the 10, namely,[14]

$$\varphi(x,y)=\tfrac{1}{2}ha\left[\cos\left[\frac{2\pi x}{a}\right]+\cos\left[\frac{2\pi y}{a}\right]\right]+h_{11}a\cos\left[\frac{2\pi x}{a}\right]\cos\left[\frac{2\pi y}{a}\right],$$

with $a=2.84$ Å, $h=0.1081$, $h_{11}=0.006$. The integration giving the Fourier component of the potential has been carried out by means of the special point method.[10].

The evolution of different beams versus incident angle in the vicinity of 53° is presented in Figs. 6 and 7. There is a strong disturbance in the HCWP case, the slope of the curve having a discontinuity at $\theta_i=\theta_{\vec{M}}$. This slope is very steep with the most strongly coupled beams (00 and $\bar{1}0$). For the ECP with $\chi=3$ $Å^{-1}$ the variation is smooth, and no singularity can be detected within an interval of 0.2° centered around $\theta_{\vec{M}}$.

DISCUSSION

The effect of multiple scattering is clearly apparent in Eqs. (6). In the t-matrix equation each diffracted amplitude is coupled to all the others by means of a sum over reciprocal-lattice vector $\vec{G}$. Each term of the sum is proportional to an integral, the integrand of which contains the t-matrix element relative to the $\vec{G}$ vector.

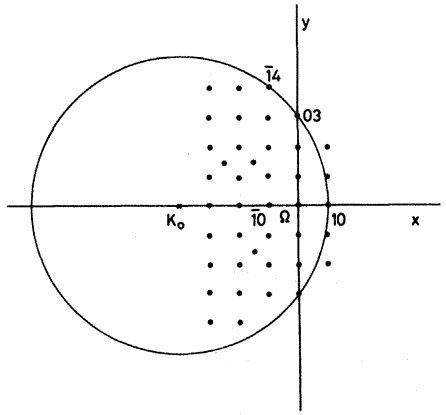

FIG. 5. Ewald diagram for He scattered by the (001) face of LiF. The incident beam is in the [110] direction, $|k_i|=11$ $Å^{-1}$, and $\theta_i=53°$.

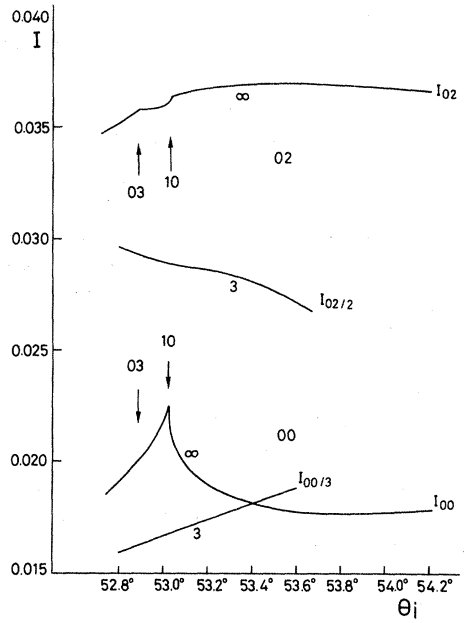

FIG. 6. Evolution of the 00 and 02 beam intensitites in the vicinity of $\theta_i = 53°$ for He with $|k_i| = 11$ Å^{-1}, incident on the (001) face of LiF. The arrows indicate the angles for which the (10) and (03) beams are emerging, $-\infty$ corresponding to the HCWP, and 3 corresponds to ECP with $\chi = 3$ Å^{-1}.

For the purpose of numerical calculation the infinte set of $\vec{G}$ vectors is truncated to a given number $N_{\vec{G}}$. Thus one retains in the calculation a finite number of Fourier components of the potential. However, when the iterative process is convergent one verifies that the unitary defect decreases as the number $N_{\vec{G}}$ increases. Therefore the generated result is close to the solution given by the full potential that would be obtained in the limit $N_{\vec{G}} \to \infty$. The effects of the neglected $\vec{G}$ vectors can be characterized by the unitary defect, which gives, roughly speaking, the precision with which intensities are calculated. In particular, the intensities that are less than the unitary defect are not significant. Fortunately, with the computers available at the present time, one can keep a sufficient number of $\vec{G}$ vectors in such a way that the unitary defect should be less than the experimental sensitivity. Thus we obtain a solution of the scattering by the full potential with a sufficient precision.

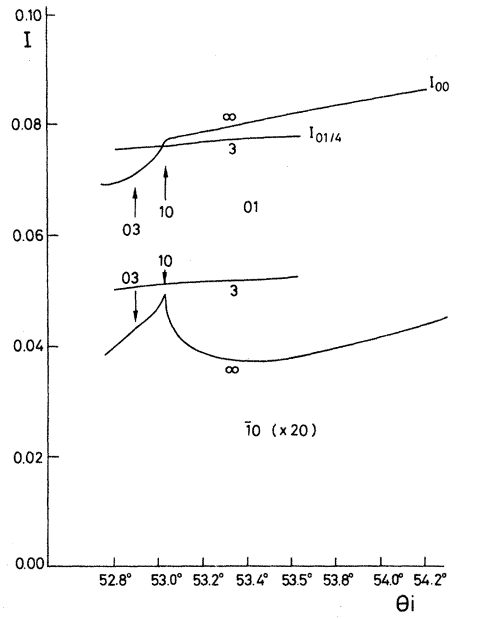

FIG. 7. Same as Fig. 6 except for the 01 and $\bar{1}0$ beam intensitities.

In order to discuss and understand on a physical basis the different results presented here it is necessary to recall that each diffracted wave is given by the product of two wave functions, namely

$$\psi_{\vec{J}}(z)\exp[i(\vec{K}_i + \vec{J})\cdot\vec{R}] .$$

The wave penetration into the potential affects only the normal component $\psi_{\vec{J}}(z)$ and therefore depends on the potential slope at an energy equal to the normal kinetic energy $e_{p_{\vec{J}}}$ of the Jth beam. For this energy the potential slope is given by

$$\frac{dV}{dz} = -\chi E_{\vec{J}_z} e_{p_i} .$$

Therefore each wave $\psi_{\vec{J}}(z)$ "feels" a potential region of different slope, and wave penetration will be higher for beams having lower normal kinteic energies.

These considerations allow one to understand the behavior of the intensities as a function of the different parameters and to predict qualitatively the effect of an ECP with respect to the HCWP. For the latter the potential slope is infinite and there is no wave penetration.

The effect of wave penetration is particularly evident in the results presented in Tables I and II. The corrugation amplitude is not too high, and multiple scattering does not play an important role. In order to see clearly this last effect we compare the variation of beams coupled to the specular beam by reciprocal-lattice vectors containing similar integers. For instance, we consider the $0\bar{1}$ and 10 beams that have $E_{\vec{J}_z}$ values equal to 1.172 and 0.604, respectively (Table I). Taking the HCWP result as reference one sees that the relative change of the intensity given by the ECP for the same χ

value is greater for the beam having the smallest $E_{\perp_z}$ value, which corresponds to a greater penetration. The same analysis can be done with the sets composed of the 11, $1\bar{1}$, and $\bar{1}\,\bar{1}$ (Table I) and of the $\bar{1}\,\bar{1}$ and $1\,\bar{1}$ (Table II). If in each set they are classed by order of increasing wave penetration, i.e., respectively $\bar{1}\,\bar{1}$, $1\bar{1}$, 11, and $\bar{1}\,\bar{1}$, $1\bar{1}$, we obtain the order of increasing intensity modifications.

The intensity variation as a function of h, the corrugation amplitude, indicates that the behavior depicted by Tables I and II holds for h values below 0.04 and 0.05 for the $\bar{1}0$, $\bar{2}\,\bar{2}$, $\bar{1}\,\bar{1}$ beams that have an $E_{\perp_z}$ value greater than 1. When $E_{\perp_z}$ is less than 1 this behavior holds until h equal approximately 0.11 for the 01, 0.15 for the $\bar{1}1$ and $\bar{2}1$, and a very large value for the 11. The shift Δh of the rainbow maxima (Table III) is between 0.014 and 0.022 and, except for the 11 beam, does not seem to be linked to the normal kinetic energy value. However, the intensity maxima I_m are directly influenced by this quantity. Comparing the I_m value for the $\bar{1}\,\bar{1}$ and $\bar{1}1$, one sees that the ECP intensity maxima for the former is greater than those given by the HCWP, the contrary being true for the latter. The same comparison can be done for the $\bar{1}0$ and 01 beams. The only beam which behaves differently is the $\bar{2}1$; this may be due to the effect of multiple scattering as its maximum appears at a high corrugation amplitude. Thus at least for the lowest $\vec{G}$ vector beam the effect of wave penetration is to enhance or reduce the rainbow intensity according to whether the penetration is lower or greater than that of the specular wave.

As far as the emerging beam phenomenon is concerned it is clear that the soft potential reduces the importance of the intensity singularities until they disappear completely. As their magnitude seems to be linked to the potential slope (χ) their measurements under conditions where the specular is as close as possible to the emerging beam can allow the determination of an approximate value of χ. This outlines their practical importance.

CONCLUSION

We have reported here a way in which the equation of a neutral particle scattered by an exponential corrugated potential can be solved without approximation to any desired accuracy. The solution is obtained by iteration of the integral-equation set with, if necessary, a translation of the distorted potential with respect to the corrugated potential. We have shown numerically that the process converges to a good solution in a sufficiently large domain of corrugation amplitudes allowing one to solve all the practical cases encountered in experimental situations.

The results compared to those given by the hard corrugated wall show the importance of the wave penetration phenomenon. When the diffracted beam intensities are plotted versus corrugation the soft potential yields a shift of the intensity maxima towards a stronger corrugation. Also it produces an enhancement or a reduction of beam intensities at the rainbow maximum according to whether the normal kinetic energy of the beam is larger or smaller than that of the specular beam. Also demonstrated is an attenuation of the singularities which appear when a beam is emerging. This last effect can be used to get an approximate value of the potential slope.

Of course these conclusions have been drawn considering numerical solutions of the t-matrix equation. Therefore they have been obtained with a well-defined particle-crystal system. Nevertheless, they certainly are valid for other systems at least in a qualitative way since they are based on the physical effect of wave penetration into the potential.

ACKNOWLEDGMENTS

The authors would like to thank Dr. C. Manus for his constant interest, and Dr. J. Lapujoulade, Dr. Y. Lejay, J. Perreau, and B. Salanon for fruitful discussions.

APPENDIX

Letting $\lambda_{00}=xy+2\lambda_{01}$, $\lambda_{01}=a^2$, $x+y=\lambda_{01}$, the product of the two matrices

$$\begin{vmatrix} x & a & & \\ a & x & a & \\ & a & x & a \\ & & & \ddots \end{vmatrix} \begin{vmatrix} y & a & & \\ a & y & a & \\ & a & y & a \\ & & & \ddots \end{vmatrix} \tag{A1}$$

gives

$$A = \begin{vmatrix} \lambda_{00}-\lambda_{01} & \lambda_{01} & \lambda_{01} & & \\ \lambda_{01} & \lambda_{00} & \lambda_{01} & \lambda_{01} & \\ \lambda_{01} & \lambda_{01} & \lambda_{00} & \lambda_{01} & \lambda_{01} \\ & & & & \ddots \end{vmatrix}, \tag{A2}$$

a matrix equal to that of the text [Eq. (14)] except for the first and last term on the diagonal. In the limit where the matrix size N is large the two matrices would have the same eigenvalues.

The determinant of A is equal to the product of the two determinants of (A1). These have been calculated[15] and one has

$$\mathrm{Det}(A)=\lambda_{01}^{N}\frac{\sin(N+1)\varphi}{\sin\varphi}\frac{\sin(N+1)\alpha}{\sin\alpha}\ ,$$

with

$$x=2\sqrt{\lambda_{01}}\cos\varphi\ ,\quad y=-2\sqrt{\lambda_{01}}\cos\alpha\ ,$$

or equivalently

$$\mathrm{Det}(A)=\prod_{1}^{N}\left\{x-2\sqrt{\lambda_{01}}\cos\left[\frac{n\pi}{N+1}\right]\times\left[y-2\sqrt{\lambda_{01}}\cos\left[\frac{n\pi}{N+1}\right]\right]\right\},$$

or

$$\mathrm{Det}(A)=\prod_{1}^{N}\left\{\lambda_{00}-2\lambda_{01}\left[1+\cos\left[\frac{n\pi}{N+1}\right]-2\cos^{2}\left[\frac{n\pi}{N+1}\right]\right]\right\}.$$

Therefore the eigenvalues are

$$\omega_n=\lambda_{00}-2\lambda_{01}\left[1+\cos\left[\frac{n\pi}{N+1}\right]-2\cos^{2}\left[\frac{n\pi}{N+1}\right]\right]$$

[1]G. Armand and J. R. Manson, Phys. Rev. Lett. 43, 1839 (1979).
[2]G. Armand, J. Phys. (Paris) 41, 1475 (1980).
[3]N. Esbjerg and J. K. Norskov, Phys. Rev. Lett. 45, 807 (1980).
[4]D. R. Hamann, Phys. Rev. Lett. 46, 933 (1980).
[5]G. G. Kleiman and V. Landman, Phys. Rev. B 8, 5484 (1973).
[6]E. Zaremba and W. Kohn, Phys. Rev. B 15, 1769 (1977).
[7]For a recent review see, H. Hoinkes, Rev. Mod. Phys. 52, 933 (1980).
[8]G. Armand and J. R. Manson, Surf. Sci. (in press).
[9]J. M. Jackson and N. F. Mott, Proc. R. Soc. London Ser. A 137, 703 (1932).
[10]B. Salanon and G. Armand, Surf. Sci. (in press).
[11]S. G. Mikhlin, *Integral Equations* (Pergamon, New York, 1964).
[12]N. Cabrera, V. Celli, F. O. Goodman, and R. Manson, Surf. Sci. 19, 67 (1970).
[13]K. L. Wolfe, D. J. Malik, and J. H. Weare, J. Chem. Phys. 67. 1031 (1977).
[14]N. Garcia, J. Chem. Phys. 67, 897 (1977).
[15]D. E. Rutherford, Proc. R. Soc. Edinburg 63A, 232 (1950).